DOI:
10.1109/TMECH.2023.3247832

Document Version
Publisher's PDF, also known as Version of record

Robot-Assisted Trans-Esophageal Ultrasound and the Virtual Admittance-Based Master-Slave Control Method Thereof

Yiping Xie, Jun Guo, Zhaokun Deng, Xilong Hou, James Housden, Kawal Rhode, Hongbin Liu, *Member, IEEE*, Zeng-Guang Hou, *Fellow, IEEE*, and Shuangyi Wang, *Member, IEEE*

***Abstract*—The robotic transesophageal ultrasound system has the potential to improve the conventional practice of diagnosis and procedure guidance that are currently performed manually. However, the existing system has obvious shortcomings in both mechanism design and safety control under remote teleoperation. This article proposed a new compact mechanism design and achieved remote teleoperation through system integration. Furthermore, this article introduced a virtual admittance-based master-slave control method that meets the needs of ultrasound operation, making the robot autonomous in regulating both force and speed. Through a series of experiments, the accuracy of the robot in operation and the effectiveness of the control method were verified. The proposed control method can regulate the contact force, slowing the increase of the interaction force to ensure safety. It can also adjust the scale of the motion automatically, allowing the user to fine tune the ultrasound plane efficiently. In addition, the controller can increase the backdrivability, avoiding injuries to the tissue due to mishandling. It is therefore concluded that work has significantly improved the usability of a transesophageal ultrasound robot and made this technology further conform to the control habits of ultrasound scanning.**

***Index Terms*—Continuum robots, master-slave control, medical robots, robotic ultrasound, robotic-assisted surgery.**

Manuscript received 29 September 2022; revised 20 December 2022 and 6 February 2023; accepted 16 February 2023. Recommended by Technical Editor F. Auat Cheein and Senior Editor H. Gao. This work was supported in part by the National Natural Science Foundation of China under Grant 62003339 and in part by the InnoHK program. *(Yiping Xie and Jun Guo are co-first authors.) (Corresponding authors: Zeng-Guang Hou; Shuangyi Wang.)*

Yiping Xie and Zhaokun Deng are with the School of Artificial Intelligence, University of Chinese Academy of Sciences, Beijing 101408, China, and also with the State Key Laboratory of Multimodal Artificial Intelligence Systems, Institute of Automation, Chinese Academy of Sciences, Beijing 100190, China (e-mail: xieyiping2020@ia.ac.cn; dengzhaokun2021@ia.ac.cn).

Jun Guo is with the Hangtian Center Hospital, Beijing 100049, China (e-mail: guojun0316@sohu.com).

Xilong Hou is with the Centre for Artificial Intelligence and Robotics, Hong Kong Institute of Science & Innovation, Chinese Academy of Sciences, Hong Kong (e-mail: xilong.hou@cair-cas.org.hk).

James Housden and Kawal Rhode are with the School of Biomedical Engineering and Imaging Sciences, King's College London, SE1 7EH London, U.K. (e-mail: richard.housden@kcl.ac.uk; kawal.rhode@kcl.ac.uk).

Hongbin Liu and Shuangyi Wang are with the State Key Laboratory of Multimodal Artificial Intelligence Systems, Institute of Automation, Chinese Academy of Sciences, Beijing 100190, China, and also with the Centre for Artificial Intelligence and Robotics, Hong Kong Institute of Science & Innovation, Chinese Academy of Sciences, Hong Kong (e-mail: liuhongbin@ia.ac.cn; shuangyi.wang@ia.ac.cn).

Zeng-Guang Hou is with the State Key Laboratory of Multimodal Artificial Intelligence Systems, Institute of Automation, Chinese Academy of Sciences, Beijing 100190, China (e-mail: zengguang.hou@ia.ac.cn).

This article has supplementary material provided by the authors and color versions of one or more figures available at https://doi.org/10.1109/TMECH.2023.3247832.

Digital Object Identifier 10.1109/TMECH.2023.3247832

I. Introduction

MEDICAL ultrasound is a valuable imaging tool that allows doctors to assess patients in real-time. An ultrasound scan is simple to perform, inexpensive, and does not involve hazardous ionizing radiation, as opposed to many other modalities. Since the late 1990s, researchers in the European Union, North America, and Japan have been interested in robotizing ultrasound devices. This was because robotized ultrasound systems could potentially address some of the drawbacks of on-site manual manipulation of hand-held probes, such as the difficulty of maintaining accurate probe positioning for long periods of time with human hands [1] and the need for experienced sonographers to be present [2]. More recently, several efforts have been made to robotize intraoperative ultrasound systems to create easier, more stable substitutes for manually controlled intraoperative ultrasound equipment [3]. Examples of intra-operative ultrasound systems include transesophageal echocardiography (TEE) and intracardiac echocardiography (ICE) for heart examination, transrectal ultrasonography (TRUS) for prostate examination, and endoscopic ultrasound for gastrointestinal tract examination.

As an early example of robotizing an intra-operative ultrasound probe, the work of Kim et al. [4] proposed a TRUS robot to assist prostate diagnosis and provide surgeons with intraoperative ultrasound navigation. The precision and accuracy of biopsy needle positioning with the assistance of the imaging robot were tested [5], and the follow-up clinical trials had proven the error is in the order of millimeters [6]. In addition to the rigid probe, flexible intraoperative ultrasound probes have also been attempted to be robotized. In contrast to rigid probes, flexible probes are soft and bendable and pass through the body's natural orifices for examination and procedure guidance. Some flexible

probes include manual controls for the distal end, i.e., the probe tip where the transducer is located. This allows the probe tip to bend relative to the long axis through cable-or wire-driven continuum mechanisms. An example of robotizing this type of probe can be found in the work of Loschak et al. The work presented an add-on four-DOF robot that can hold and manipulate an ICE catheter remotely [7]. This article series' focus was on intelligent control and navigation, e.g., auto-sweeping of multiple image planes for three-dimensional reconstruction and the automatic pointing at and imaging of targets via tracking and feedback control [8], [9].

The work of our group over the past few years has created the first trans-esophageal ultrasound robot [10] and proposed the semiautomated acquisition methodology that works with the robot [11], [12]. The overall goal was to automate TEE, a common diagnostic method for diagnosing heart disease and guiding cardiac surgical treatments. The work was motivated by the fact that the operator is required to manually hold and manipulate the TEE probe on site, which exposes them to the accompanying X-ray fluoroscopy imaging. The protection aprons are heavy and can potentially cause orthopedic injuries to the operator. Evidence suggests that up to 10% of the radiation from X-ray is still able to pass through the shielding [13]. In addition, on-site operation limits the wider utilization of this highly experience-dependent technique, as the need for highly specialized skills is always a barrier to the reliable acquisition of ultrasound. Thus, robot-assisted transesophageal ultrasound could revolutionize existing clinical practices and effectively enhance the scope of application of this device. It can keep operators away from radiation and avoid wearing heavy protective clothing, and it can also enable telemedicine for remote ultrasound and alleviate the strain on medical resources.

Despite the extensive work we have done around the TEE robot, there are still many issues with this technology toward clinical translation. First, our first-generation prototype has several problems with mechanism design and mechatronic integration, e.g., the lack of closed-loop control at the motor level and the lack of constraints on the delivery of flexible endoscopic structures at the mechanism level. Second, our first-generation prototype does not have force sensing to monitor the contact between the probe bend and the tissue, while the original probe is tactile when operated manually by manipulating the handwheels. Finally, neither our work for the TEE robot, nor the aforementioned works for other intraoperative US robots, systematically discusses how to reasonably constrain contact forces and how to achieve motion under a teleoperated master-slave control architecture. Despite having a low clinical incidence rate, complications have been widely reported [14]. These include gastric complications due to forceful retrograde of the probe in a flexion state, injuries to tissue outside the alimentary tract, and compression injuries by the probe on the branches of the posterior division of the recurrent laryngeal nerve.

The above deficiencies make it difficult to achieve clinical translation of existing work on the TEE robot. To further promote the clinical use of this robot, the following issues need to be addressed: the mechatronic design of the robot needs to be upgraded to provide improved functions required for clinical use; the teleoperation-based master-slave control needs to be investigated to ensure that the acquisition of ultrasound standard views conforms to the existing operating habits under manual operation of the conventional probe; and force control methods need to be implemented to reasonably constrain the contact force and introduce backdrivability to the system. The solution to the above problems will lay an important foundation for further clinical testing of this robot.

In this article, we aim to propose a new mechatronic design and implementation method for the TEE robot that is significantly improved over the first version regarding clinical use. Moreover, motivated by the demands of ultrasound scanning, we implemented an admittance-based master-salve control scheme for the robotic endoscopic system to ensure safe interaction and enable motion scaling. The controller would regulate the contact force between the probe tip and the tissue, slowing the increase of the interaction force to ensure safety. It would also adjust the scale of the motion when the probe tip is subjected to excessive external loads, allowing the user to adjust the ultrasound plane more efficiently and intuitively. Furthermore, the controller would also increase the backdrivability, avoiding injuries to the esophagus wall and adjacent organs due to mishandling. In the following sections, details of mechatronic design, remote operation, control scheme, and a series of validation experiments are to be presented.

II. Methods

A. Design and Implementation

A standard, manually-held commercial TEE probe is an endoscopic-like device that has four degree-of-freedom (DOF) mechanical motions operated by a trained sonographer. This includes the translation of the probe main body along the esophagus and rotation around the long axis, as well as bending the probe tip in both directions by controlling the two co-axial handwheels and the internal cable-driven continuum mechanism of the endoscope (see Fig. 1). By actively adjusting the end of the probe, the orientation of the ultrasound transducer can be controlled to examine the heart from different perspectives. Additionally, by operating two buttons on the probe or the software on the US machine, the electronic steering of the US beam can be achieved. This can be considered an additional DOF to control the US image plane, although it is not essentially necessary to be replaced mechanically when converting the hand-held probe to a motorized system.

In the proposed add-on robot, four major mechanical DOFs are motorized with customized mechanisms to manipulate a widely used Philips TEE probe (x7-2t, Philips, The Netherlands). For probes from other manufacturers, the corresponding mechanisms can be slightly adjusted to mate with the shape. As shown in Fig. 1, the robot has a set of handle control mechanisms to allow the translation, rotation, and bidirectional bending of the probe tip. These mechanisms are designed into a single unit with load-bearing supporting structures, e.g., the inner sleeve, housing, and bracket.

To control the rotation of the probe handle, the probe is fixed on the inner sleeve by the handle placement slot. The inner sleeve

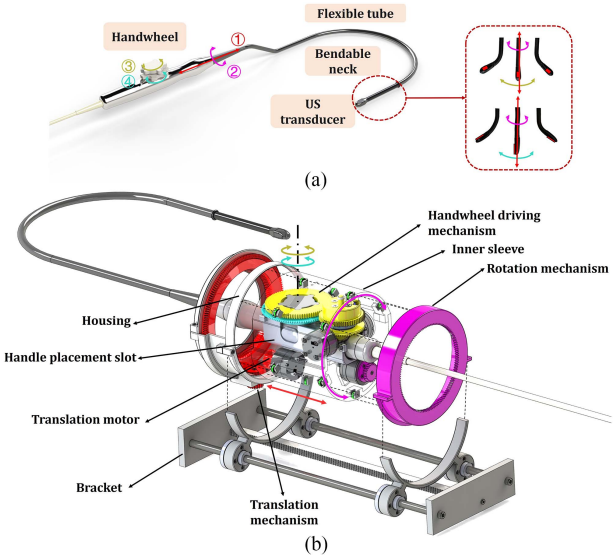

Fig. 1. Schematic representation of the original transesophageal ultrasound probe and the proposed four-DOF add-on robot.

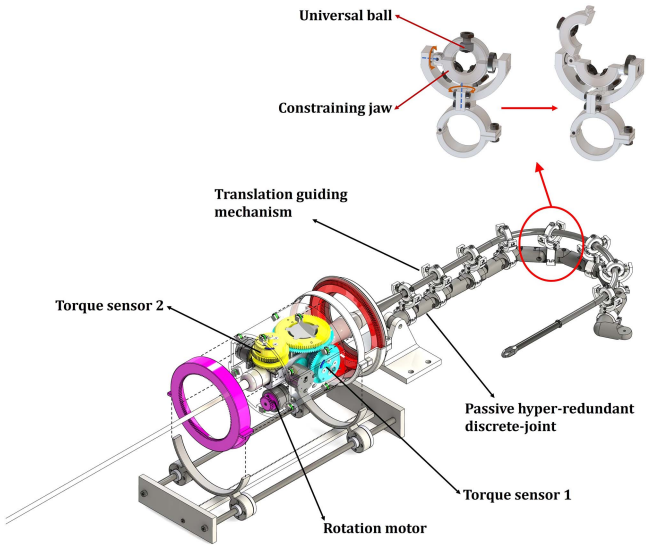

Fig. 2. Schematic representation of the translation guiding mechanism.

is supported in the housing by the miniature bearing distributed around the sleeve shell. The inner sleeve and the housing can produce relative rotation driven by the rotation motor. To control the co-axial handwheels, two gears are specially shaped to match and fixed to the handwheels. Two handwheel driving motors are mounted on both sides of the handle, and the two torque sensors are mounted on the top and side of the handle. Spur and bevel gear sets are used to transmit the motions and torques from the drive motors and torque sensors. Moreover, the housing can slide along the bracket driven by the translation motor. The rotation of the translation motor is transferred via the peripheral bevel gear and the rack and pinion mechanism to provide linear movement. Within this unit, the components are arranged in a symmetrical configuration to ensure that the center of gravity of the robot is located near the long axis, which can reduce the resistance caused by gravity when the probe rotates.

In addition, a hyper-redundant passive positioning arm with multiple discrete joints is utilized as the guiding mechanism to constrain the endoscopic portion of the probe, as shown in Fig. 2. This is required to lead the probe from the robotic system to the patient's oral cavity, which guarantees the translational movements of the robotic stage in driving the probe can be correctly transferred to the movement of the probe tip inside the patient's oral cavity and esophagus. The guiding mechanism is composed of multiple links and joints. Each joint can be controlled manually and rotated in two orthogonal directions. The length and spacing of the guiding mechanism can be adjusted according to the size and stiffness of the endoscopic portion of the probe. The constraining jaw can rotate in two orthogonal directions freely. By installing three universal balls, two DOFs that are perpendicular to the translation direction are constrained. This can effectively reduce the resistance caused by the deformation of the tube. The gravity of the translation guiding mechanism is balanced by the passive tandem manipulator, and the inflexibility is maintained by the friction between the components.

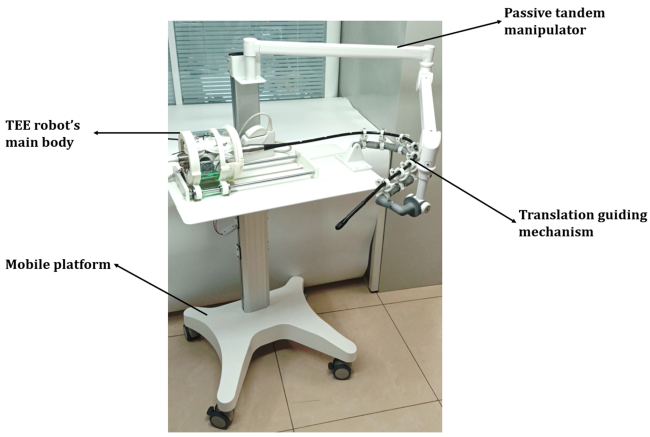

Fig. 3. Implementation of the proposed transesophageal ultrasound robot with the incorporation of its main body, mobile platform, passive tandem manipulator, and the translation guiding mechanism.

Except for standardized parts, major mechanical components were made via rapid prototyping. The robot's main part has a diameter of 160 mm and a length of 157 mm, while the bracket has a length of 445 mm. The inner sleeve of the prototype robot was made transparent to facilitate observation of the internal condition, and the outer housing was separated into left and right parts, restricted by the bracket. The implementation of the proposed TEE robot, with the incorporation of its main body, mobile platform, passive tandem manipulator, and the translation guiding mechanism, is shown in Fig. 3. To help the reader better understand our design or replicate the above robot, we have provided more detailed design drawings and videos with motion animations and real-life shots of the robot's actuation in our supplementary materials. Additionally, an executable file to show the drawing of the robot can be accessed from IEEE DataPort (doi: 10.21227/8shx-a970).

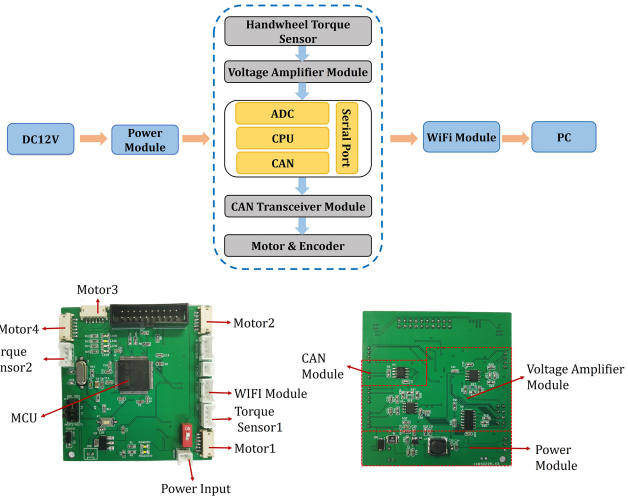

Fig. 4. Implementation details of the electronics and the custom-made board.

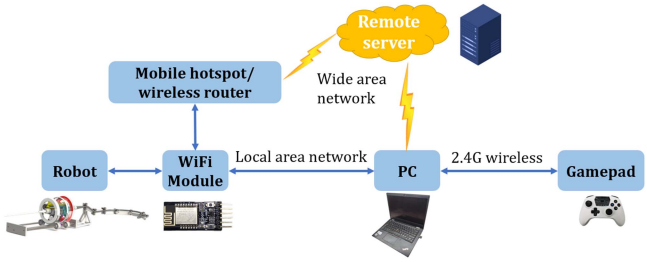

Fig. 5. Schematic diagram showing the remote operation of the robot.

B. Actuation and Remote Operation

In the proposed robot, four newly released all-in-one servo motors (RMD-L-4010, MyActuator Co., Ltd., Kunshan, China) with built-in drive and encoder are used for actuation. The motor is made with a brushless structure and can switch between open-loop, speed, and position control modes. This is regulated and can be programmed by the embedded chip on the drive (32-bit MCU, 72 MHz). The torque sensor (WTN-56, WEABU Electronics Technology Co., Ltd., Dongguan, China) is based on a bridge strain gauge, which has a measurement range of -0.3 to 0.3 N·m. In addition to the off-the-shelf components, a custom-designed circuit board (70 mm $\times$ 68 mm) is utilized for the remote operation. As shown in Fig. 4, the board includes a main control chip, a power regulating module, a voltage amplifier module, a CAN transceiver module, and a communication module. The main control chip is based on the STM32F407 series (Cortex-M4 core, 168 MHz, STMicroelectronics, Switzerland) and the communication module is based on a TTL-WIFI communication module (DT-06, Shenzhen Doctors of Intelligence & Technology Co., Ltd., Shenzhen, China).

The WiFi module enables transmission between serial and WiFi and can be easily configured with the built-in HTTP web server. With further developments, the TEE robot can work in two different modes. In the station mode, the robot can connect to a WiFi network, e.g., one created by the wireless router or a 5G hotpot. In the access point mode, the robot can create its own network and have other devices connect to it. The basic master-slave control is achieved with the use of a gamepad. The gamepad is connected to the PC with 2.4G wireless communication, allowing for position input from the sonographer and vibration feedback from the torque sensors of the robot. The overall remote-control scheme is illustrated in Fig. 5. The proposed robotic TEE probe could potentially incorporate the following scenarios using the proposed architecture.

1) The robot is in the operating room, and the sonographer is in the control room next door. A local area network (LAN) is required for the operator to remotely control the robot and stream the ultrasound images.
2) The sonographer can work in a variety of settings, including hospitals, outpatient clinics, and private homes. Both the input devices and the robot are connected to the wide area network (WAN), and data can be transferred via the remote server.

C. Force and Motion Control

The force and motion control studied in this article is strongly motivated by the clinical demands when controlling the TEE robot for cardiac diagnosis. The search for standard ultrasound views with featured anatomical structures is the most important process of the ultrasound acquisition process. For transesophageal ultrasound acquisition, the image is what the physician intends and is determined by the pose of the probe. The control of the probe tip location during this process is determined by the sonographer based on visual feedback from the image, while the speed of the probe movement and its response to contact force are primarily determined by the physician's sense of control of the handwheel. Specifically, the contact force at the probe tip is transmitted to the handwheel via the continuum mechanism, and the physician is able to sense this during the manipulation of the handwheel. A natural operation is for the physician to reduce the handwheel rotation speed as the contact force increases, avoiding excessive contact force that can cause injury to soft tissue. Moreover, when the contact force is high, it means that the physician has found the desired view and is ready to improve the quality by fine tuning. This requires a function of motion scaling by reducing the handwheel rotation speed. Considering that this type of clinical operation is performed at a low speed in a quasi-static process, the effect of acceleration is not significant.

When a robot is used to replace a physician to manipulate the TEE probe, it is necessary to have a similar response to the active operation of a physician and the perceived contact force. For medical robots, impedance and admittance-based control are widely used approaches [15], [16], [17]. For TEE acquisition, probe position is the critical element to search for the standard view and maintain image stability, while the contact force is also important to ensure the image quality and avoid tissue injury. Taking these demands into consideration, admittance-based control was investigated in our study, i.e., by measuring the interaction force with the patient, the execution

of the physician's operation can be changed through a virtual dynamics model to achieve preferred interaction responsive behavior. In this article, we focus on bidirectional bending of the probe tip and use the idea of admittance control to allow the robot's active velocity control based on force feedback by setting up a virtual dynamic model that meets the needs of clinical operation, which would coordinate with the position control dominated by the physician's master-slave operation.

The active control under force monitoring when the physician is actively operating the bending of the probe can be divided into three stages.

1) The probe tip can move freely if the contact torque is insignificant and less than the first threshold.
2) The probe tip moves in a constrained manner when the contact torque is between the first and second thresholds, indicating that the contact force has increased but is still acceptable.
3) The probe tip will be prevented from moving further if the contact torque exceeds the second threshold, indicating that the contact force is excessive.

In addition, compliance and backdrivability are the other considerations of the passive control scheme. This occurs mainly when the physician is not actively controlling the bending of the probe. For example, one of the most common processes that can result in tissue injury in manual operation is when the probe tip enters the stomach and bends, and the physician forgets to recover the bend and pulls out the probe. In order to avoid such a situation, a different virtual dynamics model is used, which is expected to result in a passive force on the probe that reverses the rotation and changes the speed depending on the interaction force when the physician does not actively control the probe bending.

As a summary, the aims of the control are as follows: to respond to the speed input and scale down the motion according to the contact force, allowing the user to adjust the ultrasound view more efficiently; to regulate the contact force between the probe tip and the tissue, slowing the increase of the interaction force via speed control to ensure safety; and to increase the backdrivability when the probe tip is not in active control, avoiding injuries to the esophagus wall and adjacent organs due to mishandling. The proposed control architecture, acting on the joint space of each bending axis, is shown in Fig. 6. The conversion between the active force-regulated controller and the passive back-driving controller is realized via monitoring whether there are inputs from the sonographer.

If the bidirectional bending is actively operated by the sonographer, then the position control is achieved by a typical master-slave configuration. The state of the probe handle $\boldsymbol{\theta}_d$ is decided by the sonographer. $\boldsymbol{\theta}_d \in \mathbb{R}^{4\times1}$ expresses the current joint space parameters of the probe handle

$$\boldsymbol{\theta} = [\theta_a, \theta_b, \theta_r, l]^T \tag{1}$$

where $\theta_a, \theta_b, \theta_r$ and $l \in \mathbb{R}$ denote the angles of handwheel for anteflex-retroflex bending (ARB) and left-right bending (LRB), the angle of handle rotation and the translation of handle, respectively. After a differential process, the expected speed change in the joint coordinate system $\dot{\Delta\boldsymbol{\theta}}$ is sent to the robot

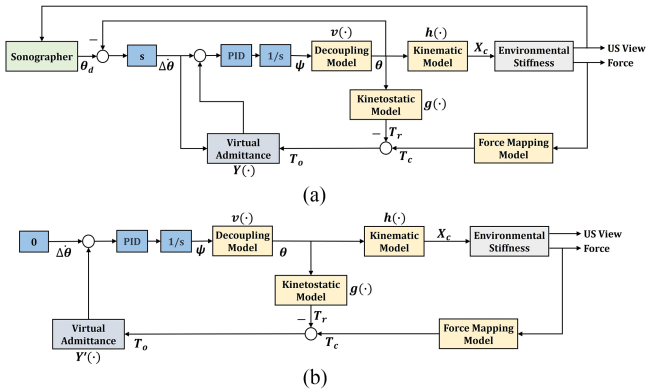

Fig. 6. Diagram of the virtual admittance control scheme under the active force-regulated and passive back-driving modes.

to avoid motion discontinuity caused by communication lags under angle control. By using a standard proportion integration differentiation (PID) controller embedded in the servo motors and one integral unit, the speed converts to the angle of each motor $\boldsymbol{\psi}$

$$\boldsymbol{\psi} = [\psi_a, \psi_b, \psi_r, \psi_l]^T \tag{2}$$

where ψ_a, ψ_b, ψ_r and ψ_l are the motor angles for ARB, LRB, rotation, and translation, respectively. The P and I parameters in the motor are set to 255 and 5, respectively. The differential parameter is determined by the controller of the motor autonomously. The decoupling process can be expressed as

$$\boldsymbol{\theta} = \boldsymbol{v}(\cdot)\boldsymbol{\psi} \tag{3}$$

$$\boldsymbol{v}(\cdot) = \begin{bmatrix} i_a & 0 & 0 & 0 \\ 0 & i_b & 0 & 0 \\ 0 & 0 & i_r & 0 \\ 0 & 0 & i_{rl} i_l & i_l \end{bmatrix} \tag{4}$$

where i_a, i_b, i_r, and i_l are the transmission ratio from motors to handle in ARB, LRB, rotation, and translation, i_{rl} is the coupling speed ratio from the rotation to the translation motor. The above parameters are related to the mechanical structure of the robot. In the prototype proposed in this article, the i_a, i_b, i_r, i_l, and i_{rl} are 1/6, 1/6, 1/5, 0.206, and 1, respectively.

The current joint space parameters $\boldsymbol{\theta}$ fed back to the angle control and result in the motion of the probe tip in cartesian space via the robot's forward kinematic model $h(\cdot)$

$$X_c = h(\theta_a, \theta_b, \theta_r, l) \tag{5}$$

where $X_c \in \mathbb{R}^{4\times4}$ is the pose and position of the probe tip represented by homogeneous matrix [10]. The interaction of the probe tip with the tissue is reflected by the environmental stiffness and ends up with the output ultrasound view and the contact force. The ultrasound view is feedback to the sonographer to guide the further adjustment. Meanwhile, the speed regulation based on the contact force is performed by the robot itself simultaneously.

The force mapping model is the relationship of the contact force from cartesian space to joint space, which is related to the internal structure of the TEE probe. Considering the cable-driven

continuum structure [18] and the decoupling characteristics between the DOFs of the TEE probe, the controller was implemented in joint space. When in action, the speed regulation is executed on the joint velocity as

$$u = Y(T_o) \tag{6}$$

$$T_o = T_c - T_r \tag{7}$$

where T_c is the measured torque on the handwheel, T_r is the torque resulting from the resistance force on the cable, and T_o is the corrected torque, which is positively correlated with the contact force between the end of the probe and the tissue. While T_c can be measured in real time, T_r is decided by the characteristics of the internal cable-driven continuum mechanism of the TEE probe. We denote this as the kinetostatic model $g(\cdot)$, which refers to the corresponding forces that are required to perform the predefined bending motion.

Directly modeling $g(\cdot)$ is difficult as the continuum mechanism parameters, e.g., modulus of elasticity, moment of the cross section of the coil part total, number of coils of the helical structure, and the coil diameter of the flexible joint, are all unknown for a commercial TEE probe. However, according to the principle of continuum mechanism, $g(\cdot)$ should be related to the joint parameters and the different tube shape configurations [19], i.e., the bending angle of the flexible part of the endoscope. Therefore, a data-based method can be used to estimate $g(\cdot)$. Polynomial is a widely used and efficient data fitting function. In this article, polynomial functions of different orders were used for fitting to evaluate their performances. Piecewise fitting was also considered for simplifying the model and improving the accuracy. In addition, a multilayer perceptron (MLP) network was implemented to fit the data for comparison. A simple and effective function would be finally selected for $g(\cdot)$ and further robot control. With both T_c and T_r available, the virtual admittance is defined based on the control state. For the virtual admittance when the sonographer is in action, i.e., actively controlling the bending

$$Y(\cdot) = \begin{cases} 0 & , \quad T_o < T_1 \\ \left(\frac{(T_o - T_2)^2}{(T_1 - T_2)^2} - 1\right)\dot{\Delta\boldsymbol{\theta}} & , \quad T_1 \le T_o \le T_2 \\ -\dot{\Delta\boldsymbol{\theta}} & , \quad T_o > T_2 \end{cases} \tag{8}$$

where Y is the speed attenuation value, T_1 and T_2 is the torque thresholds at different stages. In this article, a quadratic polynomial is used to realize motion scaling. T_1 and T_2 are 0.05 and 0.35 N·m, respectively.

When the sonographer is not in action, the expected angle $\boldsymbol{\theta}_d$ is equal to the current angle $\boldsymbol{\theta}$ and $\dot{\Delta\boldsymbol{\theta}}$ is zero. The robot performs autonomous back-driving according to another virtual admittance to ensure safety

$$Y'(\cdot) = -\frac{V}{1 + e^{-k(T_o - T_3)}} \tag{9}$$

where Y' is the back-drive speed. A sigmoid function is used to guarantee the continuity and smoothness of the speed. V, k, and T_3 are the parameters to regulate the back-drive characteristic. V is the maximum speed, k is the coefficient to adjust the equivalent acceleration, and T_3 is related to the critical torque.

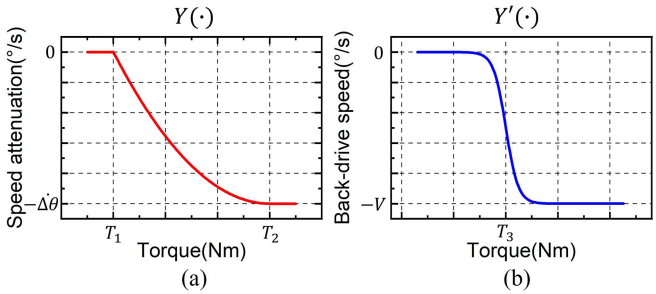

Fig. 7. Proposed virtual admittance for the controller. (a) Active state when the sonographer is in action and (b) passive state when there is no input.

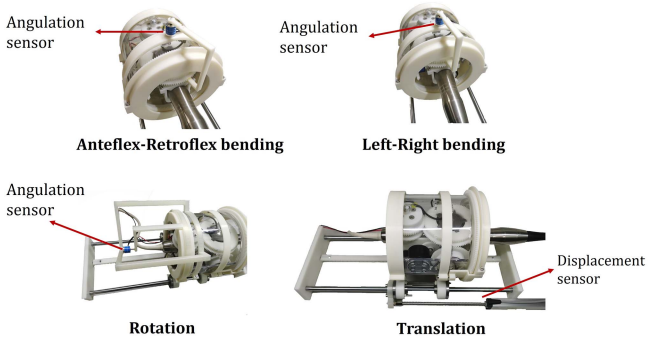

Fig. 8. Experimental setup for the accuracy test for each axis of the robot.

V, k and T_3 are 50°/s, 85, and 0.17 N·m in this article. Due to the different direction of internal sliding friction increment of cable under active bending and passive back-driving, the contact force transmission model from cartesian space to joint space is different. Under the same probe tip contact force, the torque perceived on the handwheel is lower under back-driving. Therefore, the set critical torque under back-driving mode is lower than under master-slave mode.

The designed virtual admittance is illustrated in Fig. 7, representing the expected dynamics based on the abovementioned clinical needs. In the state where the sonographer has active input for bending, the response function of the virtual admittance is characterized in terms of speed attenuation because the overall speed can also be regulated by the physician. In the state when there is no input for bending, the speed is set to specific values.

III. Experimental Validation

A. Accuracy

This section aims to perform the foundational measurements to assess the positioning accuracy of the robot. Since the error caused by the internal continuum mechanism of the commercial TEE probe cannot be eliminated, the accuracy assessment focused on the impact of the robot structure and basic motor actuation. In the experiment, four DOFs of the robot were tested using the experimental setup shown in Fig. 8. During the experiment, the respective mechanisms were connected to an independent

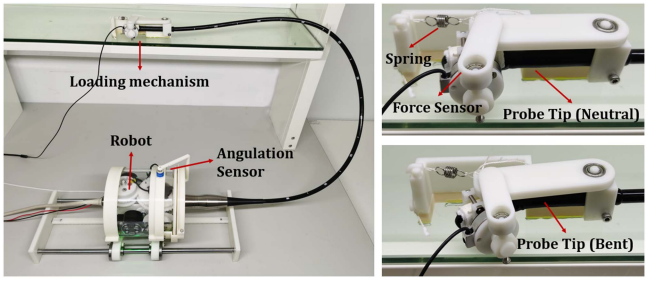

Fig. 9. Experimental setup to validate the force regulation and motion scaling.

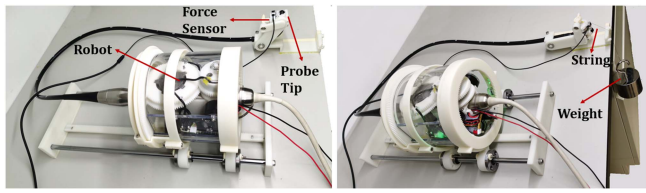

Fig. 10. Experimental setup to validate the compliance and backdrivability.

angular or translational sensor. The input is the joint parameters sent to the robot, while the output is the values detected by the attached independent sensors, which are the corresponding handwheel rotation angles for left-right and ARB, the actuation angle of the inner sleeve for rotation, and the displacement of the bracket for translation. The motor movement adopted a cyclic method, including both forward and reverse motions, to obtain the overall accuracy performance of the robot.

B. Telecommunication

This section aims to test the latency under both LAN and WAN conditions. During the LAN experiment process, the host PC connected to the WiFi and set up the server. The WiFi module utilized in the robot established a client and tried to connect to the server. The experimental condition was that the computer was 10 meters away from the WiFi module, replicating the two-way communication condition between the operating room and the surgical room. After the connection was established, the host sent out the test data and recorded the current time. The data was transferred to the WiFi module and was sent to an additional slave PC via the serial port. Then, the data was returned back to the host, and the host would record the receiving time after performing data verification. During the WAN experiment process, the WiFi module was connected to a 5G hotspot, established a client and tried to connect to the remote server. The data transmitted to the remote server would be transferred directly to the host. The procedure of the experiment was the same as for the LAN experiment.

C. Force Regulation and Motion Scaling

This section aims to present the experimental validation method to test the proposed controller regarding the force regulation and motion scaling, referred to the admittance control method presented in Section II-C. To simulate the force interaction between the probe tip and the surrounding tissue, e.g., the esophagus wall, a passive loading mechanism (see Fig. 9) with a revolute joint, a spring, and a force sensor (six-axis, M3552B, Sunrise Instruments, Shanghai, China) was designed. The force sensor was fixed at the tip of the probe. One end of the mechanism was connected to the spring tension device, and an angulation sensor was fixed onto the robot to detect the joint motion output, i.e., the handwheel's rotation angle. This mechanism, with the probe distal end inserted, was to simulate the effect that the tip contact force would increase when the probe tip actively bends, while at the same time accurately measuring the force with the mounted force sensor. During the experiment, we used the ARB axis to validate the controller. The handwheel was actuated robotically to bend the probe tip at a constant input speed. With the interaction force increasing, the admittance controller will regulate the speed, which will then influence the increasing ratio of the force and cause the effect of motion scaling. The output joint motion and torque, along with the tip force, were recorded during the experiment. Furthermore, to demonstrate the effect of the controller, a comparative experiment with no control was performed. The data was recorded for analysis.

D. Compliance and Backdrivability

This section aims to present the experimental validation method to test the proposed controller regarding the compliance and backdrivability, referred to the admittance control method presented in Section II-C. This controller is designed to introduce compliance to the probe tip when the sonographer is not actively controlling the bending motion, improving the safety of interaction, and avoiding potential mishandling. To passively introduce external forces to the probe tip, e.g., to simulate retracting the probe when it is in the stomach and already bent, an active loading mechanism (see Fig. 10) with a revolute joint, a string, and a force sensor was designed. The force sensor was fixed at the tip of the probe. The mechanism can be actuated with weights applied to the string, and the joint motion output was detected by recording the corresponding drive motor angle. This mechanism, with the probe distal end inserted, was to simulate the effect that the external force has applied to the probe tip while the probe tip is not actively controlled. During the experiment, the probe tip was bent first, and a weight was applied and then released from the mechanism. With the interaction force increasing, the admittance controller will reverse the joint motion while regulating the speed, which will then introduce the compliance and achieve backdrivability. The output joint motion and torque, along with the applied tip force, were recorded during the experiment. The data was recorded for further analysis.

IV. Results

A. Accuracy

The experimental results of the accuracy test are shown in Fig. 11. The motion errors of the ARB, LRB, rotation, and translation, expressed as the absolute mean and standard deviation, are: 0.37±0.42°; 0.17±0.21°; 0.12±0.15°; and 0.82±0.86 mm,

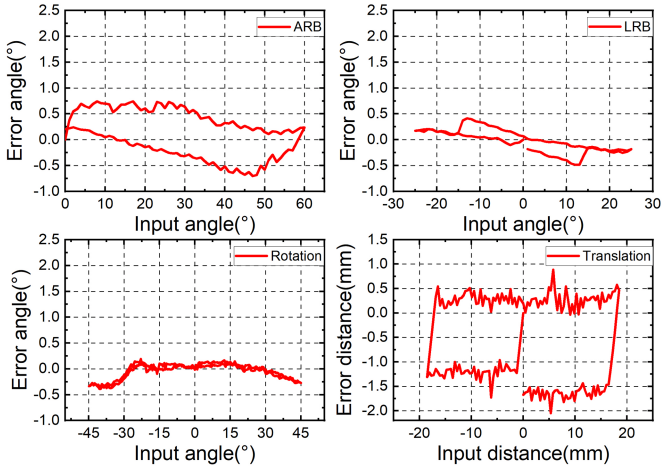

Fig. 11. Accuracy test results for the four axes of the robot.

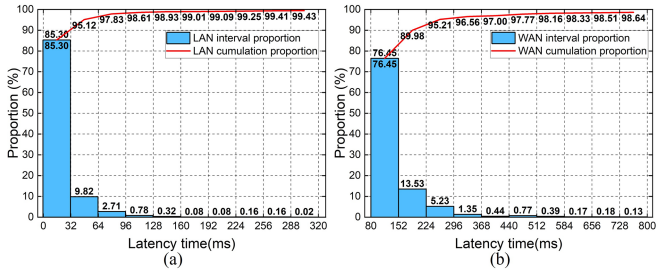

Fig. 12. Latency test results of the telecommunication under remote operation.

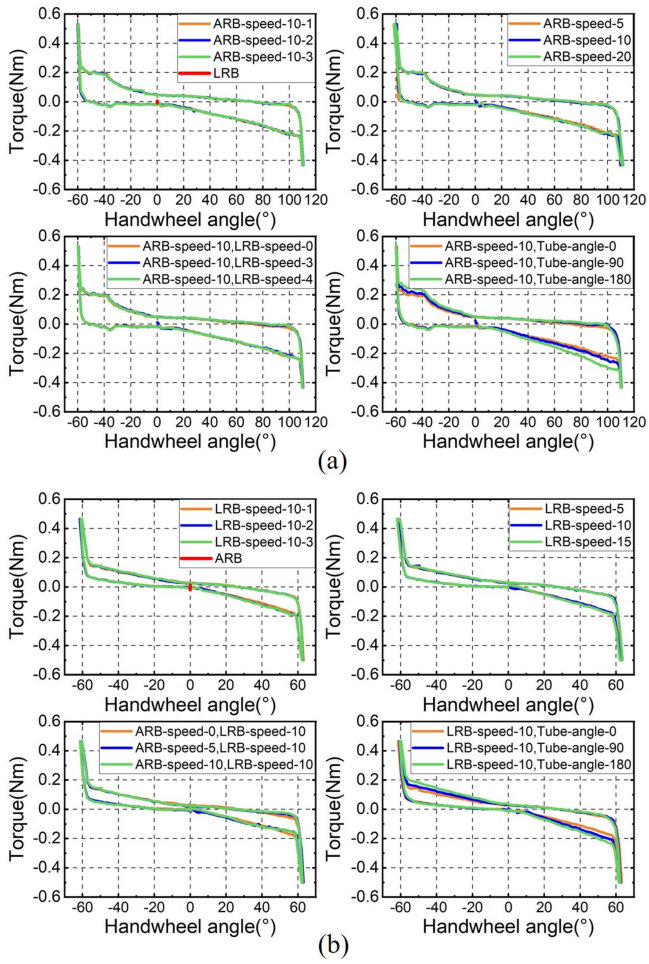

Fig. 13. Kinetostatic behavior of the probe's internal continuum mechanism. (a) Anteflex-retroflex bending ARBand (b) left-right bending axes, tested with different speeds and probe shape configurations.

respectively. Since the above accuracy test was done by cyclic reciprocating motion, Fig. 11 also shows the hysteresis effect caused by the mechanism itself. It can be seen that the errors and hysteresis effects of the LRB and rotation axes are relatively small, while the ARB and translation axes exhibit relatively larger motion errors and more obvious hysteresis effects.

B. Telecommunication

Communication latency tests with ten thousand samples of data were performed. The recorded communication delay histogram is shown in Fig. 12. The experimental results in LAN show that the mean latency is 30 ms, the maximum value is 4.75 s, and the minimum value is 6.2 ms. 99.44% of the results are less than 500 ms and 90% of the results are below 41 ms. The experimental results under WAN show that the average latency is 153 ms. The maximum value is 3.01 s, and the minimum value is 81.7 ms. 97.6% of the results are less than 500 ms and 90% of the results are below 224 ms. It should be noted that the test data is the delay of two-way communication. When considering the one-way transmission delay between the master and the slave devices, the latency is half of the value theoretically. The results of the communication experiments show that the overall latency for telecommunication is not significant considering the TEE acquisition is non-invasive, though there are minor lags that need to be optimized.

C. Internal Resistance Calibration

The measurement outcomes of the kinetostatic behavior of the probe's internal continuum mechanism, i.e., the relationship between the driving torque of the handwheels and the rotation angle executed at different speeds and with different probe shape configurations, are shown in Fig. 13.

Overall, the above T–D relationship demonstrates a clear hysteresis performance, i.e., the resistance to be overcome to produce motion varies for the same handwheel rotation angle as the handwheel is turned forward and backward. We further analyzed this kinetostatic characterization from different perspectives. The example of repeatability testing demonstrates that the characteristics during probe bending are highly reproducible. The characteristics at different knob speeds also indicate that there is no significant difference at different speeds. Additionally, the crosstalk effect was also investigated with the results shown in Fig. 13. It can be found that the motion of the LRB in the nonlimit position has no significant effect on the required actuation torque of the ARB, and vice versa. However, as shown in Fig. 13, under different tube shape configurations, there are some changes in the internal actuation torque. In this experiment,

TABLE I
COMPARISON OF DIFFERENT FITTING MODELS

	ARB standard error (Nm)	LRB standard error (Nm)
Quadratic polynomial	5.233×10^{-3}	2.43×10^{-3}
Cubic polynomial	4.174×10^{-3}	2.085×10^{-3}
Quartic polynomial	3.767×10^{-3}	1.993×10^{-3}
Quintic polynomial	3.594×10^{-3}	1.942×10^{-3}
Six-time Polynomial	3.507×10^{-3}	1.907×10^{-3}
MLP Network	3.084×10^{-3}	2.423×10^{-3}

shape configurations with the tube bent at approximately 0° and 180° were tested.

Considering the above experimental measurements, we modeled the kinetostatic effect of the probe by fitting five polynomial functions of different orders and a four-layer MLP network. The piecewise fitting strategy was used to determine the variation of internal resistance characteristics for the polynomial functions. The number of nodes in each layer of the network is 2, 5, 10, 10, 1. The training sample is less than 250 sets of data. The batch size is 32. The learning rate is 0.008 and it changes to 0.001 when the loss for a batch size is lower than 2×10^{-5}. The training times are one hundred thousand. The comparison of different fitting model standard errors is given in Table I.

By analyzing the data, the fitting standard error was found to be less than 1% of the entire range when the order of polynomial is greater than two. According to the results of ARB and LRB, the speed of the decreases for standard error slows down gradually when exceeding the cubic polynomial. In this article, considering the simplification and precision of fitting function, a cubic polynomial is used to model the internal resistance characteristics, which is expressed as

$$g'(\cdot) = a\theta^3 + b\theta^2 + c\theta + d \tag{10}$$

where θ is the angle of handwheel, a, b, c, and d are the coefficients to be fitted. Due to the change of internal resistance resulting from different angle configurations of the tube, a quadratic polynomial compound function related to tube angle and handwheel angle is used for compensation. The kinetostatic model $g(\cdot)$ is

$$g(\cdot) = g'(\cdot) + \left(f\varphi^2 + g\varphi\right)(\theta + e) \tag{11}$$

where φ is the tube-configurated angle and e, f, g are the coefficients to be fitted. Table II gives the values of fitting parameters. The fitting results under different tube configurations are shown in Fig. 14.

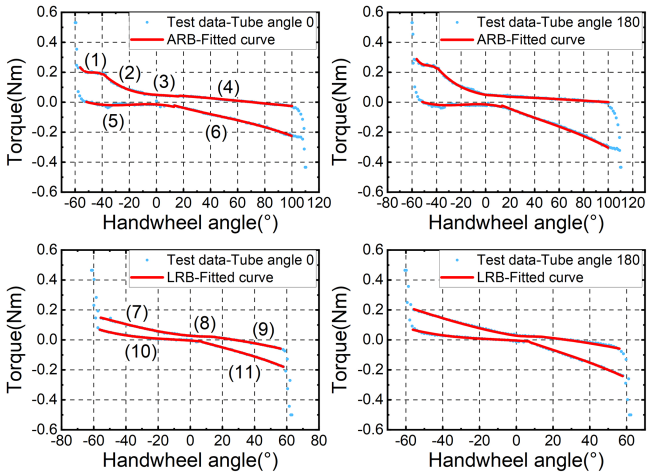

Fig. 14. Calibration results of the internal resistance of the probe's mechanisms.

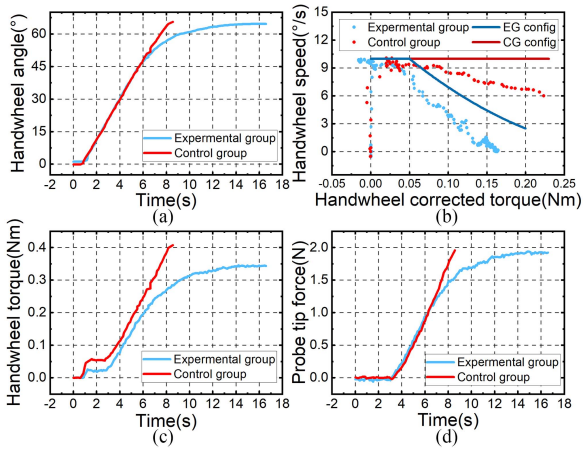

Fig. 15. Experimental results of the motion scaling and force regulation. (a) Handwheel motion regulation, (b) Handwheel speed regulation. (c) Handwheel torque regulation. (d) Probe tip force regulation.

D. Motion Scaling and Force Regulation

The results of the action of the admittance control on the motion and force are shown in Fig. 15. The control group only uses position control mode. For the regulation of the handwheel rotation speed, Fig. 15(a) shows the variation of the handwheel angle with time, and it can be seen that the growth rate is gradually decreasing in the experimental group. The increase in time corresponds to the change in the contact force. Fig. 15(b) further shows the relationship between the handwheel rotation speed and the measured torque. Compared with the designed virtual model, the measured torque-velocity curve shows the same trend as the preset model, although the specific measured value of the velocity change differs from the preset. In general, when the contact force is small, the speed remains unchanged. When the contact force reaches the first threshold, the handwheel rotation speed starts to decrease, which will realize the desired motion scaling effect. This will allow the operator to adjust the position of the probe with higher precision to find the optimal US view. Fig. 15(c) and (d) shows the results of the force regulation. The perceived torque on the handwheel and the contact force at the tip show a linear increase when the admittance controller is not active. With the virtual dynamics model enabled using the admittance control, the growth rate of both the contact force and the torque on the handwheel gradually decreases and tends to zero. This will allow a safe interaction between the probe and the tissue.

E. Backdrivability and Compliance

The results of the action of the admittance control on backdrivability and compliance are shown in Fig. 16. The control group

TABLE II
PARAMETERS USED IN THE FITTED KINETOSTATIC MODEL

Section	Angle range (°)	a	b	c	d	e	f	g
(1)	(-56, -40)	-4.336×10^{-5}	-6.107×10^{-3}	-2.866×10^{-1}	-4.282	0	-4.8×10^{-4}	-5.2×10^{-4}
(2)	(-40, 0)	-1.258×10^{-6}	2.377×10^{-5}	-6.791×10^{-4}	4.914×10^{-2}	0	-4.8×10^{-4}	-5.2×10^{-4}
(3)	(0, 34)	-1.258×10^{-6}	2.377×10^{-5}	-6.791×10^{-4}	4.914×10^{-2}	0	0	0
(4)	(34, 100)	2.662×10^{-8}	-5.81×10^{-6}	-4.703×10^{-4}	5.316×10^{-2}	-34	-1.6×10^{-4}	5.6×10^{-4}
(5)	(-50, 13)	-8.707×10^{-7}	-4.805×10^{-5}	-4.784×10^{-4}	-1.456×10^{-2}	0	0	0
(6)	(13, 100)	-1.517×10^{-7}	2.034×10^{-5}	-2.903×10^{-3}	1.35×10^{-2}	-13	-6×10^{-4}	-3×10^{-4}
(7)	(-55, 0)	1.79×10^{-7}	3.257×10^{-5}	-9.139×10^{-4}	2.792×10^{-2}	0	0	-1×10^{-3}
(8)	(0, 17.3)	1.79×10^{-7}	3.257×10^{-5}	-9.139×10^{-4}	2.792×10^{-2}	0	0	0
(9)	(17.3, 55)	-4.41×10^{-8}	-8.191×10^{-6}	-1.11×10^{-3}	3.794×10^{-2}	0	0	0
(10)	(-55, 6)	-3.857×10^{-7}	-1.18×10^{-5}	-7.295×10^{-4}	-4.193×10^{-3}	0	0	0
(11)	(6, 55)	-2.907×10^{-7}	1.379×10^{-5}	-3.07×10^{-3}	8.21×10^{-3}	-6	0	-1.2×10^{-3}

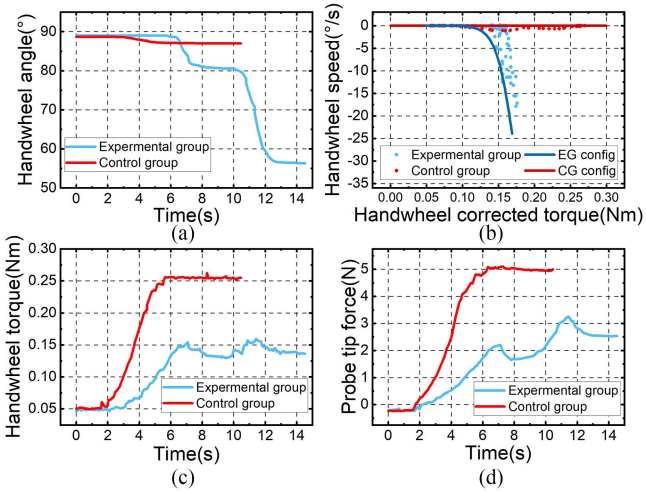

Fig. 16. Experimental results of the backdrivability and compliance. (a) Handwheel motion regulation. (b) Handwheel speed regulation. (c) Handwheel torque regulation. (d) Probe tip force regulation.

only uses position control mode. The effect of backdrivability is illustrated by the responsive change in handwheel rotation angle over time, as shown in Fig. 16(a). According to the virtual dynamics of this state, the increase in passive force would lead to an increase in reversal speed, which is verified by the measured results, as shown in Fig. 16(b). This process dynamically regulates the relationship between contact force and reversal speed to achieve the change of compliance and backdrivability. When the passive force acting on the end of the bent probe exceeds the set threshold, the admittance controller starts to regulate the probe speed and drives the handwheel into reverse. Compared with the control group, it can be found that the admittance controller proposed in this article can effectively introduce compliance to both the handwheel and the probe tip, as shown in Fig. 16(c) and (d).

V. DISCUSSIONS

This article introduces the design of an add-on robotic system to assist transesophageal ultrasound acquisition with a four-DOF main actuation unit, a mobile platform, a passive tandem manipulator, and a hyper-redundant passive guiding mechanism. In terms of its flexibility in practical use, this is a major improvement over our previous system reported in [10]. Furthermore, to provide safe interaction and motion scaling, we established an admittance-based master-salve control scheme, which was prompted by the demands of remote-operated ultrasound scanning. The controller would regulate the contact force between the probe tip and the tissue, slowing the increase of the interaction force to ensure safety. When the probe tip is subjected to high external loads, it adjusts the scale of the motion, allowing the user to alter the ultrasound plane more efficiently and intuitively. In addition, the controller would improve backdrivability, preventing mishandled injuries to the tissue. To our knowledge, our work is the first to investigate these important issues, provide domain knowledge-based solutions for force regulation and motion scaling, and systematically report the experimental results for an add-on intra-operative ultrasound robot, when compared with the existing works [7], [10], [20], [21].

As can be seen from the experimental results of the accuracy test, the ARB and translation axes exhibit relatively larger motion errors and more obvious hysteresis effects. This is mainly due to the imperfection of the mechanical structure. The main reasons are the internal clearance and material deformation of the mechanism. More specifically, the main reasons for the *ARB* axis are the backlash and deformation due to the fixation of the drive gear shaft, as well as the gap between the probe handwheel and the force sensor engagement gear. The main reason for the error in the translation axis is the gap caused by the gear-rack meshing. The above problems can be optimized by improving the integrated design of the drive chain, adjusting the gear design parameters, including the error compensation function in the software, and adjusting the handle fixing structure.

The experimental results related to the admittance control are in accordance with the model expectations and can meet the required capabilities of force constraints, motion scaling, and backdrivability with and without inputs from the physician. The active controller meets the expected performance in that it will slow the increase of the interaction force to ensure safety when pressurizing the tissue and slow the drive speed when contact force increases to allow the sonographer to adjust the position of

the probe with higher precision. The passive controller meets the expected performance that it will introduce active compliance and allow backdrivability of the probe tip when it is subjected to external force, e.g., forcefully retract the probe tip from the stomach when it is already bent.

Specific analysis of the results reveals that the actual controlled speed is always less than the set speed, and the error gets larger as the handwheel torque increases. The possible reason is that the PID controller used for the motor speed regulation is still not the best, which makes the output speed lower than the set speed when it is subjected to external forces. Our future work will further optimize the motor control to achieve a better speed following effect. In addition, we will also consider predicting the contact force at the probe tip and using the force information in Cartesian space to further improve the safety of the operation. We will also consider designing a bespoke haptic input device for more intuitive control.

VI. Conclusion

This article proposed a new design method for the transesophageal ultrasound robot. The basic remote operation function was realized through a telecommunication architecture. Considering human-machine collaboration and safe interaction, this article also proposed a virtual admittance model for master-slave control and explored the force and velocity input-output relationships to achieve soft-smooth interaction, motion scaling, and backdrivability. The above work has significantly improved the usability of a transesophageal ultrasound robot and makes this technology further conform to the control habits and operating intentions of ultrasound scanning.

References

[1] N. Magnavita, L. Bevilacqua, P. Mirk, A. Fileni, and N. Castellino, "Work-related musculoskeletal complaints in sonologists," *J. Occup. Environ. Med.*, vol. 41, no. 11, pp. 981–988, Nov. 1999.

[2] L. LaGrone, V. Sadasivam, A. Kushner, and R. Groen, "A review of training opportunities for ultrasonography in low and middle income countries," *Trop. Med. Int. Health*, vol. 17, no. 7, pp. 808–819, Jul. 2012.

[3] A. M. Priester, S. Natarajan, and M. O. Culjat, "Robotic ultrasound systems in medicine," *IEEE Trans. Ultrason. Ferroelect. Freq. Control*, vol. 60, no. 3, pp. 507–523, Mar. 2013, doi: 10.1109/TUFFC.2013.2593.

[4] C. Kim, F. Schäfer, D. Chang, D. Petrisor, M. Han, and D. Stoianovici, "Robot for ultrasound-guided prostate imaging and intervention," in *Proc. IEEE/RSJ Int. Conf. Intell. Robots Syst.*, Dec. 2011, pp. 943–948.

[5] M. Han et al., "Geometric evaluation of systematic transrectal ultrasound guided prostate biopsy," *J. Urol.*, vol. 188, no. 6, pp. 2404–2409, Dec. 2012.

[6] S. Lim, C. H. Jun, D. Y. Chang, D. Petrisor, M. Han, and D. Stoianovici, "Robotic transrectal ultrasound guided prostate biopsy," *IEEE. Trans. Biomed. Eng.*, vol. 66, no. 9, pp. 2527–2537, Sep. 2019, doi: 10.1109/TBME.2019.2891240.

[7] P. M. Loschak, A. Degirmenci, Y. Tenzer, C. Tschabrunn, E. Anter, and R. D. Howe, "A four degree of freedom robot for positioning ultrasound imaging catheters," *J. Mech. Robot.*, vol. 8, no. 5, pp. 510161–510169, Aug. 2016.

[8] P. M. Loschak, L. J. Brattain, and R. D. Howe, "Automated pointing of cardiac imaging catheters," in *Proc. Int. Conf. Robot. Autom.*, 2013, pp. 5794–5799.

[9] P. M. Loschak, A. Degirmenci, C. M. Tschabrunn, E. Anter, and R. D. Howe, "Automatically steering cardiac catheters in vivo with respiratory motion compensation," *Int. J. Rob. Res.*, vol. 39, no. 5, pp. 586–597, Feb. 2020.

[10] S. Wang, J. Housden, D. Singh, K. Althoefer, and K. Rhode, "Design, testing and modelling of a novel robotic system for trans-oesophageal ultrasound," *Int. J. Med. Robot. Comput. Assist. Surg.*, vol. 12, no. 3, pp. 342–354, Sep. 2016.

[11] S. Wang, D. Singh, D. Johnson, K. Althoefer, K. Rhode, and R. J. Housden, "Robotic ultrasound: View planning, tracking, and automatic acquisition of transesophageal echocardiography," *IEEE Robot. Autom. Mag.*, vol. 23, no. 4, pp. 118–127, Dec. 2016, doi: 10.1109/MRA.2016.2580478.

[12] S. Wang et al., "Robotic intra-operative ultrasound: Virtual environments and parallel systems," *IEEE/CAA J. Autom. Sinica*, vol. 8, no. 5, pp. 1095–1106, May 2021, doi: 10.1109/JAS.2021.1003985.

[13] E. F. McIlwain et al., "Radiation safety for the cardiac sonographer: Recommendations of the radiation safety writing group for the council on cardiovascular sonography of the American society of echocardiography," *J. Amer. Soc. Echocardiography*, vol. 27, no. 8, pp. 811–816, Aug. 2014.

[14] J. N. Hilberath, D. A. Oakes, S. K. Shernan, B. E. Bulwer, M. N. D'Ambra, and H. K. Eltzschig, "Safety of transesophageal echocardiography," *J. Amer. Soc. Echocardiography*, vol. 23, no. 11, pp. 1115–1127, Nov. 2010.

[15] A. Calanca, R. Muradore, and P. Fiorini, "A review of algorithms for compliant control of stiff and fixed-compliance robots," *IEEE/ASME Trans. Mechatron.*, vol. 21, no. 2, pp. 613–624, Apr. 2016, doi: 10.1109/TMECH.2015.2465849.

[16] C. Ott, R. Mukherjee, and Y. Nakamura, "Unified impedance and admittance control," in *Proc. Int. Conf. Robot. Autom.*, 2010, pp. 554–561.

[17] C. Yang, G. Peng, Y. Li, R. Cui, L. Cheng, and Z. Li, "Neural networks enhanced adaptive admittance control of optimized robot–Environment interaction," *IEEE Trans. Cybern.*, vol. 49, no. 7, pp. 2568–2579, Jul. 2019, doi: 10.1109/TCYB.2018.2828654.

[18] K. P. Ashwin, S. K. Mahapatra, and A. Ghosal, "Profile and contact force estimation of cable-driven continuum robots in presence of obstacles," *Mechanism Mach. Theory*, vol. 164, Oct. 2021, Art. no. 104404.

[19] L. Ott, F. Nageotte, P. Zanne, and M. de Mathelin, "Robotic assistance to flexible endoscopy by physiological-motion tracking," *IEEE Trans. Robot.*, vol. 27, no. 2, pp. 346–359, Apr. 2011, doi: 10.1109/TRO.2010.2098623.

[20] C. Pahl, H. Ebelt, M. Sayahkarajy, E. Supriyanto, and A. Soesanto, "Towards robot-assisted echocardiographic monitoring in catheterization laboratories usability-centered manipulator for transesophageal echocardiography," *J. Med. Syst.*, vol. 41, no. 11, Sep. 2017, Art. no. 148.

[21] S. M. Sajadi, K. Mathiassen, H. Brun, and O. J. Elle, "Design, kinematic modeling, and validation of a robotic-assisted transesophageal echocardiography system," in *Proc. IEEE/SICE Int. Symp. System Integr.*, 2022, pp. 250–257, doi: 10.1109/SII52469.2022.9708810.

Yiping Xie received the B.Eng. degree in mechanical engineering from Beihang University, Beijing, China, in 2020. He is currently working toward the M.Sc. degree with the School of Artificial Intelligence, University of Chinese Academy of Sciences and the Institute of Automation, Chinese Academy of Sciences, Beijing, China.

His research interests include mechatronics design, robot control, and human-robot interaction.

Jun Guo received the Bachelor's degree in medicine from Tianjin Medical University, Tianjin, China, in 1993 and the Master's degree in medicine from Peking University Health Science Center, Beijing, China, in 2006.

From July 2009 to July 2017, she was an Associate Professor with Peking University Health Science Center and has been a Professor since August 2017. She is currently the Executive Vice President of Internet Hospital of Hangtian Medical and Health Technology Group Co., LTD., the Vice President of Hangtian Center Hospital, and the Academic leader of ultrasound. Her specialty is ultrasound diagnostics.

Zhaokun Deng received the B.Eng. degree in automation from Beihang University, Beijing, China, in 2021. He is currently working toward the M.Sc. degree with the School of Artificial Intelligence, University of Chinese Academy of Sciences and the Institute of Automation, Chinese Academy of Sciences, Beijing, China.

His research interests include mechatronics design, robot control, and human-robot interaction.

Xilong Hou received the B.Eng. and M.Eng. degrees in mechanical engineering from Northeastern University, Shenyang, China and Harbin Institute of Technology (Shenzhen), Shenzhen, China, in 2012 and 2015, respectively.

He was an Engineer in ROBO medical, Peng Cheng laboratory and Shenzhen Institute of Artificial Intelligence and Robotics for Society. He is currently a Senior Engineer with the Centre for Artificial Intelligence and Robotics (CAIR), Hong Kong institute of Science and Innovation, Chinese Academy of Science, Beijing China. His research interests include medical robotics and robot-assisted surgery.

James Housden received the B.A. and M.Eng. degree in engineering and the Ph.D. degree in ultrasound imaging from the Department of Engineering, the University of Cambridge, Cambridge, U.K. in 2004 and 2008, respectively.

Since 2011, he has been with the School of Biomedical Engineering and Imaging Sciences, King's College London, and is currently a Senior Teaching Fellow. His research interests include ultrasound imaging, interventional imaging and biomedical robotics.

Kawal Rhode received the Bachelor's degree in basic medical sciences and radiological sciences from Guy's & St. Thomas' Hospitals Medical School, London, U.K., in 1992 and the Doctorate degree in medical physics from the Department of Surgery, University College London, London, U.K., in 2006.

Since 2001, he has been with the School of Biomedical Engineering and Imaging Sciences, King's College London, and is currently Professor of Biomedical Engineering and Head of Education. His current research interests include image-guided interventions, intelligent mechatronics systems for interventions and ultrasound imaging, 3D printing in healthcare and pedagogy for biomedical engineering.

Hongbin Liu (Member, IEEE) received the B.E. degree from Northwestern Polytechnic University, China, in 2005, the M.Sc. degree in mechatronics and the Ph.D. degree in robotics from King's College London, UK, in 2006 and 2010, respectively.

He is a Reader in medical robotics with the School of Biomedical Engineering and Imaging Sciences, Faculty of Life Sciences and Medicine, King's College London, London, U.K. He is the Director of Haptics Mechatronics and Medical Robotics Laboratory, Centre for Robotics Research. His research lies in creating soft and compliant robots with appropriate haptic perception to elegantly and safely interact with changing and unstructured environment, at the same time, enhancing the understanding of the environment through the haptic interaction. His research interests include haptic sensing of medical instruments, haptic sensing and control for steerable catheters and endoscopes for medical intervention and diagnosis, and robotic ultrasound manipulation.

Zeng-Guang Hou (Fellow, IEEE) received the B.E. and M.E. degrees from Yanshan University, Qinhuangdao, China, in 1991 and 1993, respectively, and the Ph.D. degree from Beijing Institute of Technology, Beijing, China, in 1997, all in electrical engineering.

From May 1997 to June 1999, he was a Postdoctoral Research Fellow with the Key Laboratory of Systems and Control, Institute of Systems Science, Chinese Academy of Sciences, Beijing, China He was a Research Assistant with the Hong Kong Polytechnic University, Hong Kong, from May 2000 to January 2001. From July 1999 to May 2004, he was an Associate Professor with the Institute of Automation, Chinese Academy of Sciences, and has been a Full Professor since June 2004. He is currently the Deputy Director of the State Key Laboratory of Management and Control for Complex Systems, Institute of Automation, Chinese Academy of Sciences, Beijing, China. His research interests include neural networks, robotics, and intelligent systems.

Shuangyi Wang (Member, IEEE) received the B.Eng. and Ph.D. degrees in biomedical engineering from Tianjin University, Tianjin, China, in 2013 and King's College London, London, U.K., in 2017, respectively.

From 2017 to 2020, he was a Research Associate with the School of Biomedical Engineering and Imaging Sciences at King's College London. He is currently an Associate Professor with the Institute of Automation, Chinese Academy of Sciences, China. His research interests include medical robotics, robotic ultrasound, and robot-assisted surgery.